OBSERVATIONS FOR VALIDATING CUMULUS PARAMETERIZATIONS

Richard H. Johnson
Colorado State University
Fort Collins, Colorado, USA

Summary: Temperature, moisture and cloud distributions in the tropics are reviewed. Important perturbations in the temperature and moisture profiles are detected at two levels in the troposphere: (1) between 2 and 3 km in association with the tradewind inversion and (2) near the 0°C level (~ 5 km), apparently in association with melting in convective systems. In the western Pacific warm pool region, three distinct cloud populations are found: tradewind cumulus, cumulus congestus (topping out in the midtroposphere just above the 0°C level) and deep cumulonimbus.

1. INTRODUCTION

Broadly speaking, approaches for the parameterization of cumulus convection in large-scale models can be classified into two general categories: moist-convective adjustment and schemes based on cloud models. Both approaches typically assume that the atmosphere tends to adjust toward some equilibrium thermodynamic state following the imposition of large-scale destabilization; however, the net impacts of the parameterized convection on the large-scale flow are scheme-dependent. The success of parameterizations can be measured by the realism of these impacts and, ultimately, prediction skill; however, since models contain other parameterizations (e.g., boundary layer, microphysics, radiation, etc.), assessment of impact on skill can be fraught with difficulties.

The most basic properties of the flow that can be used to validate cumulus parameterization are temperature, moisture, wind, vertical motion and cloud fields. In a broad sense, distributions of temperature, moisture and clouds are reasonably well known. Remarkably, however, there are important details which are still quite uncertain. Many of these details are related to the wide-ranging effects of cumulus convection. For example, accurate observations of upper-tropospheric water vapor are notably lacking. Therefore, the validation of parameterized cumulus effects on upper-level moisture fields cannot be readily accomplished, yet this moisture field, which is heavily influenced by cirrus detrainment from cumulonimbus, plays a critical role in the atmospheric radiation budget.

Temperature and diabatic heating errors in the tropics associated with deficiencies in cumulus parameterizations can translate directly to errors in large-scale circulation features; the Hadley and Walker cells, monsoonal flows and the zonal mean circulations, as has been discussed by Albrecht et al. (1986) and others. In addition, cumulus parameterization schemes, even if not reproducing them directly, must properly represent the effects of distinct and prominent cloud populations such as the tradewind cumulus, since these play an essential role in atmospheric heat, moisture, momentum, radiation budgets and consequently the large-scale circulation. This overview has an emphasis on results from the 1992-93 TOGA COARE (Tropical Ocean Global Atmosphere Coupled Ocean-

Atmosphere Response Experiment, Webster and Lukas 1992), since that experiment has shed new light on issues relating to cumulus parameterizations.

2. THERMODYNAMICS

2.1 Temperature

The gross features of the temperature profile in the tropics can be described quite well by radiative-convective equilibrium. Temperature changes in the tropics are small ($\leq$ 0.5K), and it can be argued that these that do occur are primarily associated either with convective circulations interacting with boundaries or radiative effects. To illustrate this, temperature perturbations for the GATE Phase III easterly wave composite of Thompson et al. (1979) are shown in Fig. 1. Since the composite is for

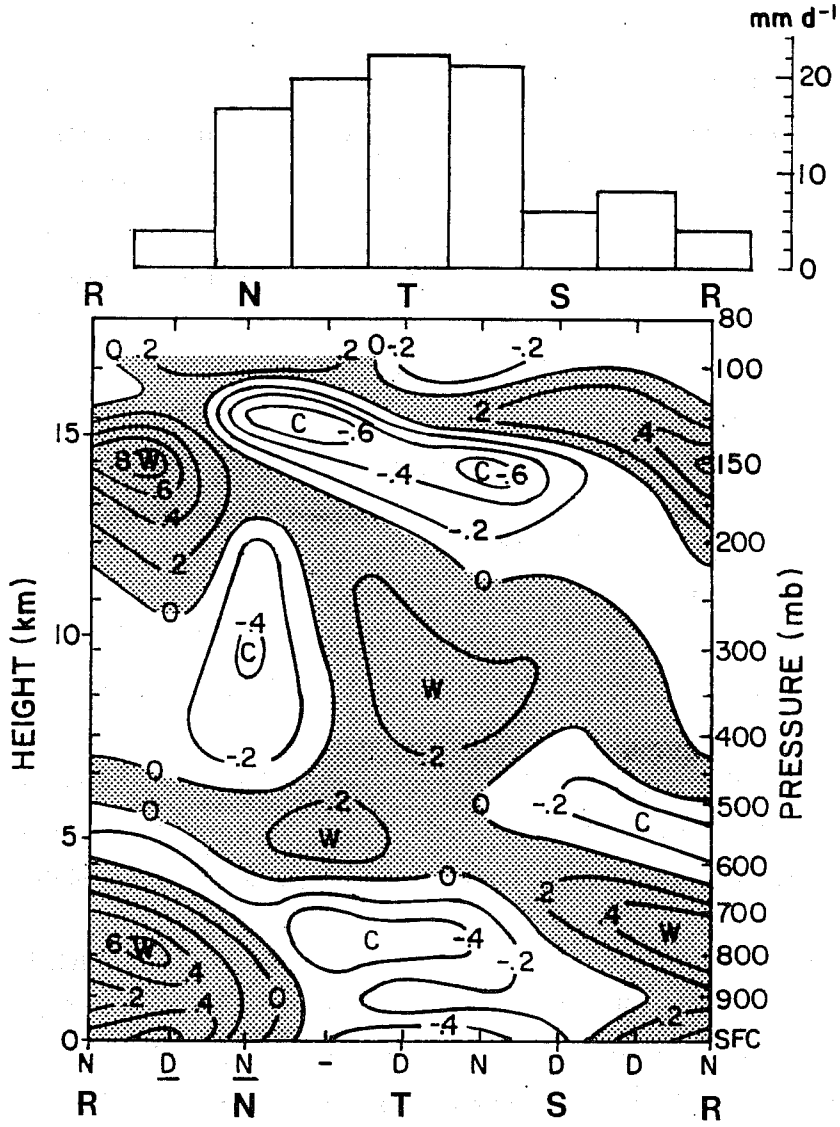

Figure 1: Precipitation (top) and temperature deviations (°C, bottom) for composite easterly wave (from Thompson *et al.* 1979). **R**, N, **T** and **S** refer to wave ridge, axis of northerly flow, trough and axis of southerly flow, respectively. N and D refer to a preference for night and day soundings, respectively, with underline indicating an extreme preference of one over the other.

a limited period of 20 days, there is an unequal diurnal distribution of soundings in the eight wave categories. Wave categories which had a predominance of daytime sounding releases are denoted by D and those at night by N (underline indicates an extreme occurrence of one over the other).

The African easterly waves are a strong modulator of precipitation, such that there was five times the rainfall in the trough as in the ridge (Fig. 1) Three primary perturbations in the temperature field (all < 0.7 K) were observed in the trough, also noted in a composite of west Pacific easterly waves (Reed and Recker 1971): (1) near-surface cooling associated with downdrafts from deep convection, (2) mid- to upper-tropospheric warming associated with latent heat release and (3) near-tropopause cooling, presumably associated with overshooting cumulonimbus tops. The largest of these perturbations, (1) and (3), are a result of circulations within deep convection impinging on the lower and upper boundaries of the troposphere.

There is also a prominent cooling near 750 mb (2.5 km) in the wave trough, which at first glance might be attributed to cooling by downdrafts. However, further examination shows that this feature is an indirect manifestation of lower-tropospheric warming associated with the broad stratiform regions of squall lines that occurred in the wave ridge. Payne and McGarry (1977) showed that these squall lines formed ahead of the wave trough (in the region of northerly flow or category **N** in Fig. 1), moved faster than the easterly wave itself and dissipated near or just before reaching the wave ridge. The warming, which is commonly observed at low levels near the back edge of trailing stratiform regions of squall lines, is a manifestation of dynamical processes associated with mesoscale organization of convection. Strong system-relative rear-inflow jets can form to the rear of these systems due to strong buoyancy gradients within them. Overshooting of descending rear-inflow jets appears to be the mechanism responsible for the lower-tropospheric warming and drying that produces "onion-shaped" soundings (Zipser 1977). Diagnostic studies of such systems in Winter MONEX indicate that while the net forcing at low levels by the diabatic processes of melting and evaporation in the stratiform regions is a cooling, the response is just the opposite: a warming (Fig. 2, from Johnson 1986). Since Fig. 1 illustrates departures from the wave mean, the cooling near 750 mb in the wave trough, rather than a direct response to convective processes there, is more accurately interpreted as a manifestation of convectively induced low-level warming near the wave ridge.

In addition to the direct effects of convection, some of the temperature anomalies in Fig. 1 may be a consequence of the unequal diurnal distribution of observations. Most of Wave Category 1 (between **R** and **N**) soundings were taken during the day, whereas most of Category 2 (**N**) soundings were at night. The strong warming (about 1°K) near 150 mb in Category 1 may be a reflection of shortwave absorption at high levels (Randall et al. 1991). The pronounced shift from column-integrated warming in the Category 1 (between **R** and **N**) to cooling in Category 2 (**N**) is in large part a consequence of predominantly daytime (Category 1) vs. nighttime (Category 2) soundings.

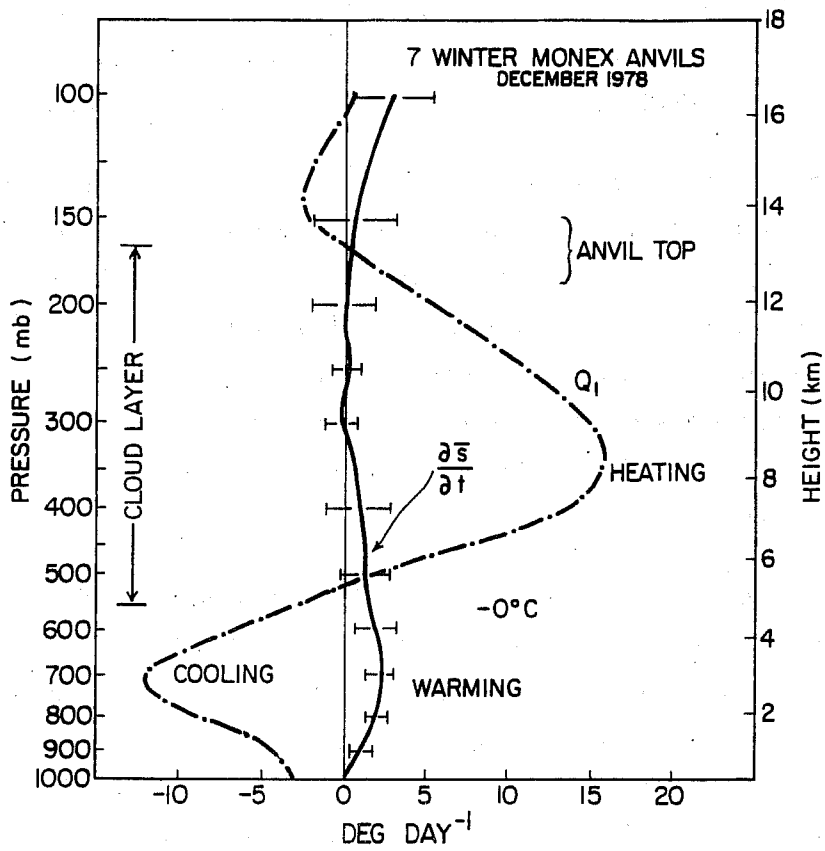

Figure 2: Composite storage of dry static energy ($\frac{\partial \bar{s}}{\partial t}$) and heating rate Q_1 for seven Winter MONEX mesoscale anvils. Horizontal bars indicate standard deviation. From Johnson (1986).

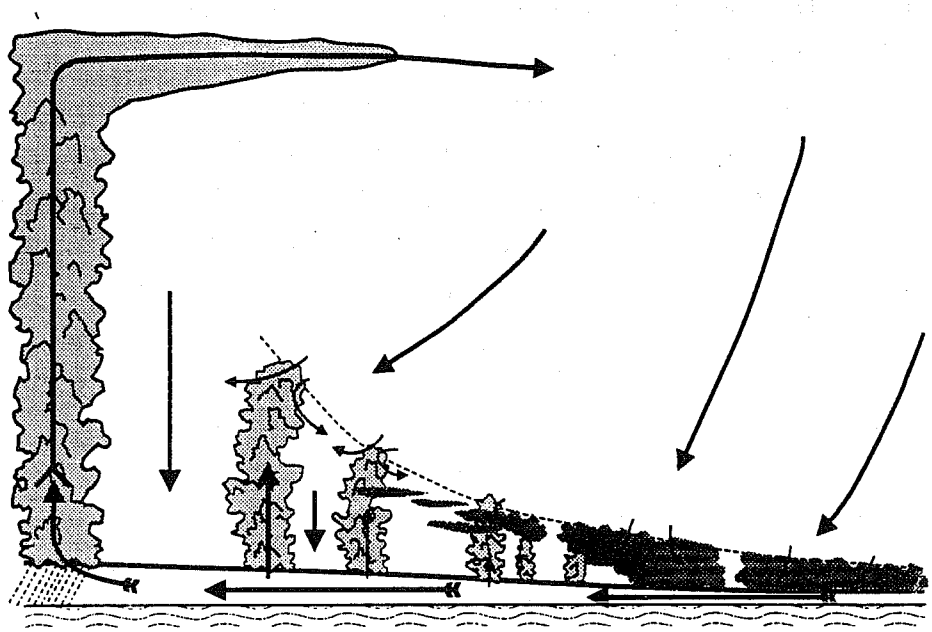

Figure 3: Hypothesized structure of the tropical atmosphere, showing the various regimes, approximately as a function of sea surface temperature (from Emanuel 1994).

If global models are to realistically represent cloud populations or their effects, then the tradewind cumulus layer must be taken into account. It has traditionally been argued that the depth of this layer is controlled thermodynamically, i.e., by a balance between surface buoyancy flux and large-scale subsidence, such that its depth increases toward the equator as SST increases and subsidence decreases (Fig. 3). However, recent reanalysis of Atlantic data (Schubert et al. 1994) and results from the western Pacific (Johnson et al. 1993) indicate that rather than gradually increasing in depth toward the ITCZ, the tradewind inversion is more often than not quasi-horizontal throughout the tropics until meeting up with the ITCZ. An example of this structure in the western Pacific is shown in Fig. 4. In this case on 4 November 1992, relative humidity data from TOGA COARE show

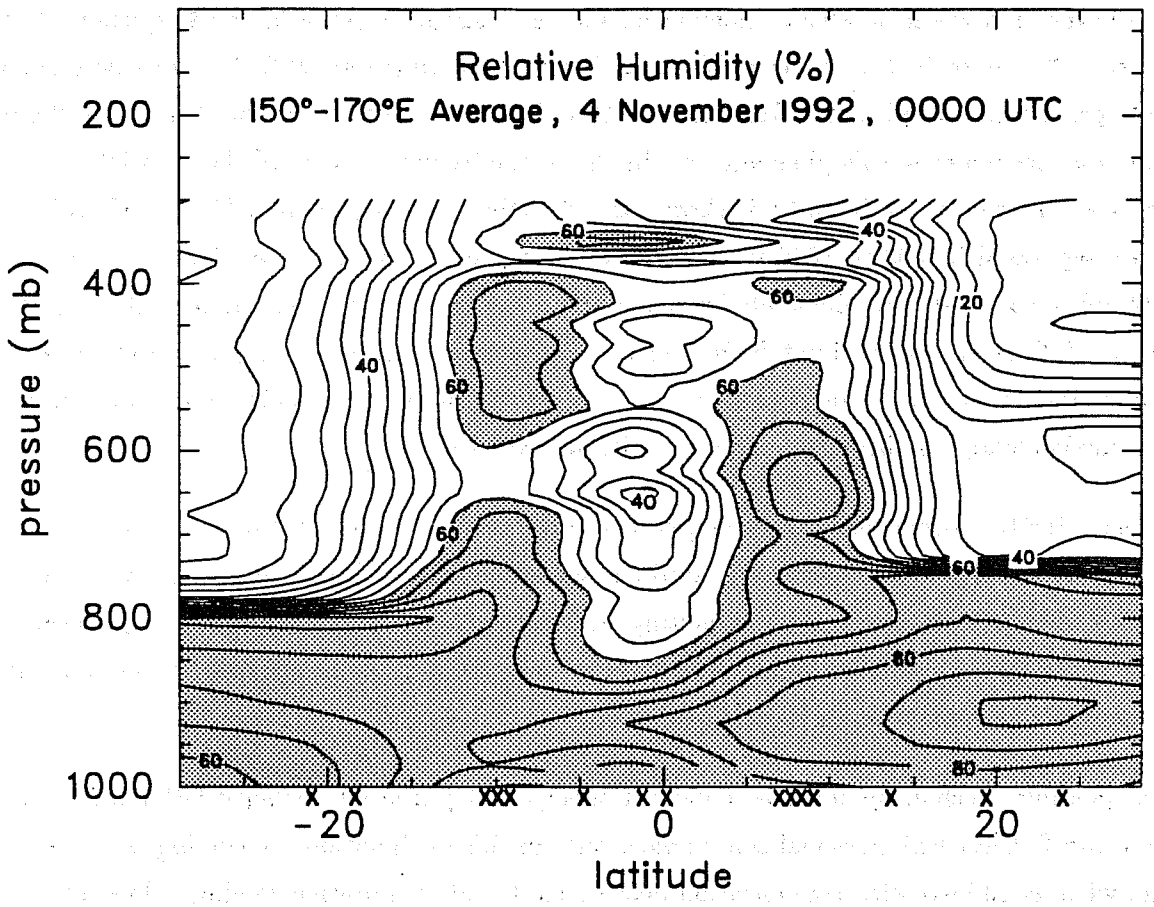

Figure 4: North-south cross-section of relative humidity (%) in the longitude band 150-170°E for 4 November 1992, 0000 UTC. X's indicate positions of sounding sites.

sharp, quasi-horizontal trade inversions between 800 and 700 mb poleward of two ITCZs north and south of the equator. It has been recently shown by Schubert et al. (1994) that such behavior can be explained by resorting to dynamical, as opposed to thermodynamical arguments. By formulating a generalization of the Rossby adjustment problem, they show that the trade inversion layer tends to be quasi-horizontal extending toward the equator. The trade inversion height is controlled by horizontally averaged (over a Rossby length or more) values of sea-surface temperature, divergence

and above-inversion atmospheric structure, but since the Rossby length becomes very large toward the equator, dynamical constraints exert a more dominant control there, spreading the structure at subtropical latitudes horizontally toward the equator.

The prevalence of a trade inversions in the eastern Atlantic is illustrated in a contoured frequency vs. altitude diagram (CFAD) for Porto Santo (33.1°N, 16.3°W) which shows a distinct maximum in the frequency of stable layers between 800 and 850 mb (Fig. 5a). The same diagram for Kapingamarangi (1.0°N, 154.5°E) in the western Pacific, though nearly on the equator, shows a similar increase in stability near 800 mb reflecting the presence of a trade inversion there, although it is less prominent (Fig. 5b). An additional peak near 925 mb corresponds to the inversion atop the surface mixed layer. Another feature in the Kapingamarangi plot is a slight increase in the frequency of stable layers near 500 mb, or just above the 0°C level. While a seemingly small feature in this format, an alternate procedure that plots the frequency of stable layers exceeding a certain threshold illustrates the common occurrence of this phenomenon. In Fig. 6 the frequency of stable layers with lapse rates greater than or equal to -4 K km^{-1} is shown as a function of height at four TOGA COARE sites, which are separated by 500 to 1000 km and more. Two primary peaks are evident at each site: one near 800 mb associated with the trade inversion and a lesser, but still prominant peak near 550 mb or near the 0°C level. Approximately 20% of the soundings taken during COARE exhibited stable layers of at least this magnitude near this level. The stable layers were typically observed in mostly clear or partly cloudy conditions outside precipitation regions.

Mechanisms for the formation of the temperature inversions near the 0°C level are unclear at this time. One possibility is that they are residual isothermal layers from decayed convection. Such layers are known to exist just below the melting level in stratiform rain regions (e.g., Findeisen 1940). However, many stable layers are observed to develop apart from from pre-existing convection, thereby requiring another explanation in those cases.

Another possible mechanism involves balanced theory and potential vorticity (PV) inversion (W. Schubert and P. Ciesielski, personal communication). In this explanation the cooling associated with melting, when combined with condensation heating aloft and evaporative cooling below, produces a strong vertical gradient in the diabatic heating rate ($\dot{\theta}$). Mass is removed from the isentropic layers near the melting level, thereby creating a local positive PV anomaly (e.g., Raymond and Jiang 1990). When this anomaly is inverted to obtain the associated balanced wind and mass fields, a horizontal spreading effect occurs, resulting in a temperature inversion in regions horizontally distant from the melting.

Yet another explanation invokes gravity waves, although their net effect is uncertain due to transience, mean flow effects and other factors. In particular, heat sources resembling those associated with tropical cloud clusters generate internal gravity waves, referred to by Mapes (1993) as "buoyancy

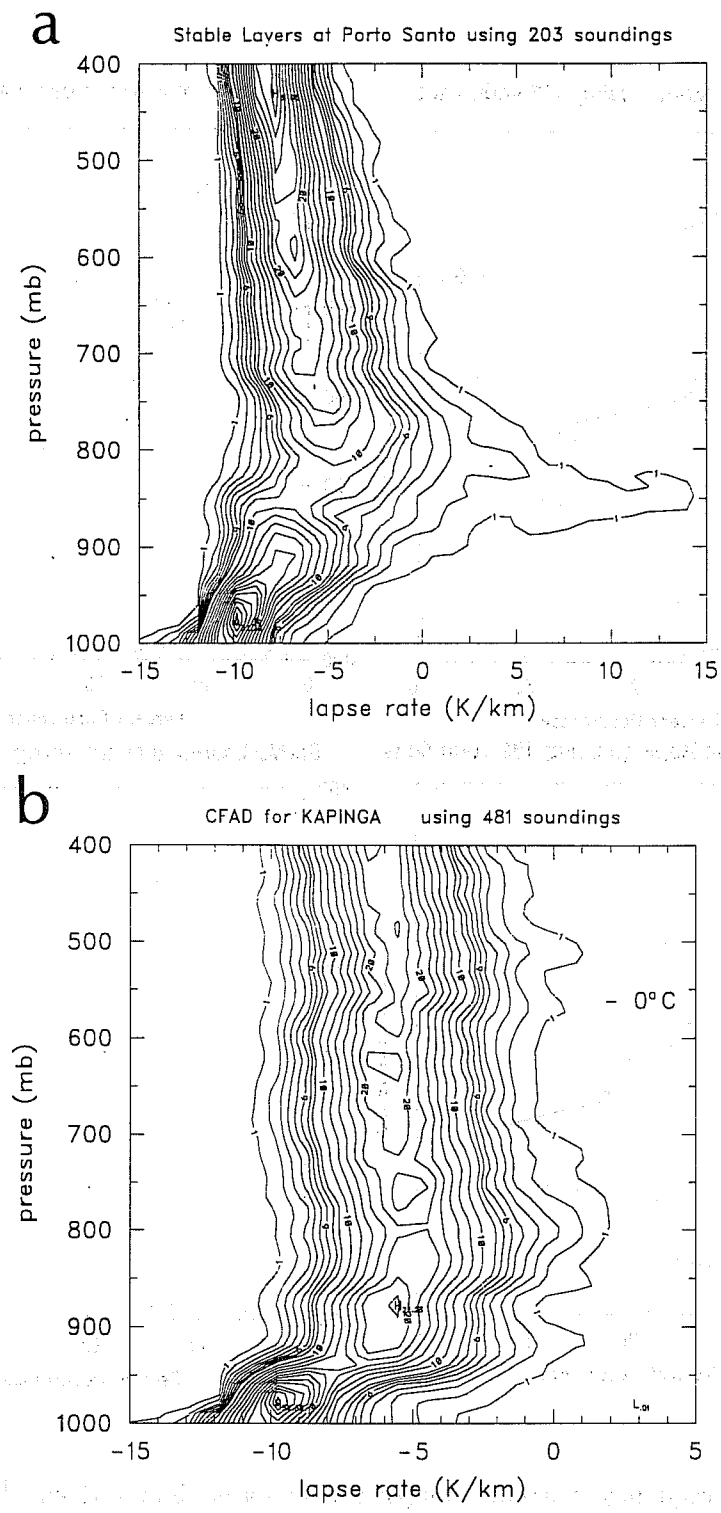

Figure 5: Sounding statistics for high-resolution soundings at (a) Porto Santo Island (33.1°N, 16.3°W) from 1 to 28 June 1992 and (b) Kapingamarangi (1.0°N, 154.5°E) from 1 November 1992 to 28 February 1993. Isolines of frequency (percent) of observations at a particular level which have lapse rates in a 1 K km^{-1} size bin; note that the contour interval is 1% for low frequencies and 2% for frequencies higher than 8%.

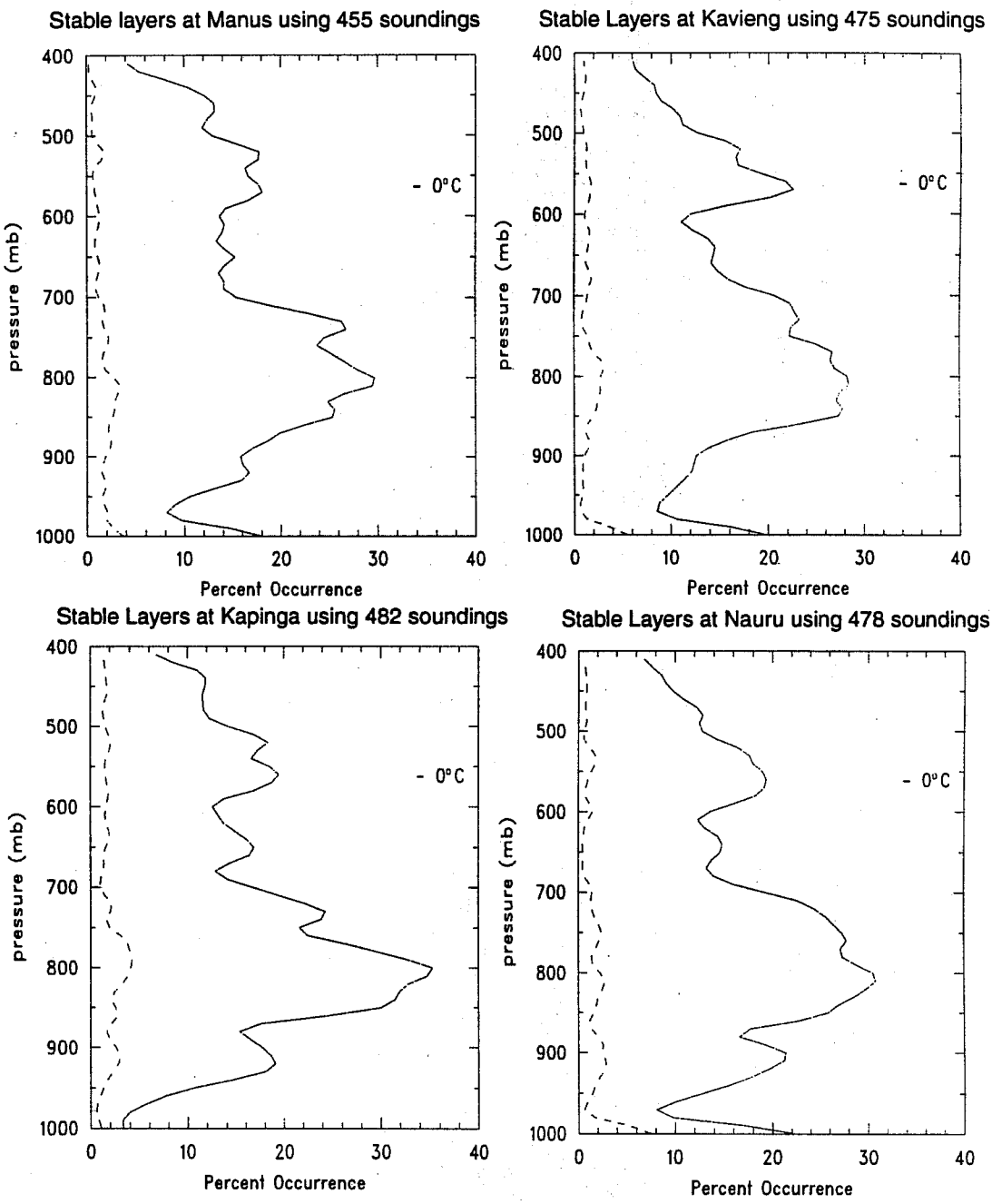

Figure 6: Cumulative frequency (percent) of lapse rates greater than -4 K km^{-1} (solid curve) and 0 K km^{-1} (dashed curve) for Manus (2.0°S, 147.3°E), Kavieng (2.4°S, 150.5°E), Kapingamarangi (1.0°N, 154.5°E) and Nauru (0.3°N, 166.6°E) for the four-month period November 1992 - February 1993.

bores," that produce sinking aloft and ascent at low levels outside the convection, which can increase stability at midlevels (Nicholls et al. 1991).

Data from the TOGA COARE shipboard radars reveal a connection between the cloud population statistics and the temperature profile observations. The frequency distribution of echoes stratified by top height recorded by the MIT radar aboard the R/V *Vickers* (2.1°S, 156.3°E) for the period 10 November - 10 December 1992 (Fig. 7, from T. Rickenbach, personal communication) shows two

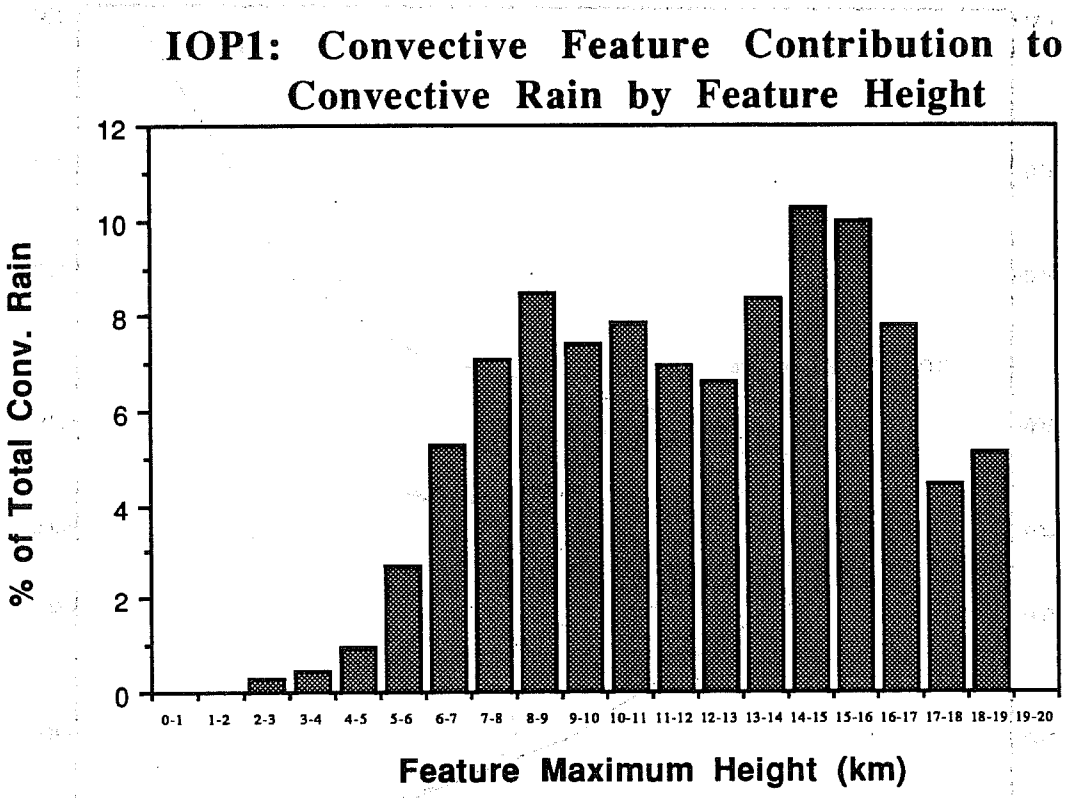

Figure 7: Percent contribution to total convective rainfall by clouds having tops in various height ranges as measured by MIT radar aboard R/V *Vickers* for period 10 November - 10 December 1992 (courtesy T. Rickenbach).

peaks: one in the upper troposphere (14-16 km) associated with deep convection and the other in the midtroposphere (7-9 km). The latter peak may be a reflection of the aforementioned frequently occurring stable layers near the 0°C level which would serve to limit cloud growth. The 0°C level is near 5 km, but growth to 7-9 km may be a result of overshooting. Similar bimodal distributions of cloud-top height were observed during GATE (Cheng and Houze 1979).

2.2 Humidity

As mentioned earlier, a notable deficiency of present sounding systems is their inability to accurately measure water vapor in the upper troposphere. During TOGA COARE a special effort was made to correct for this deficiency by employing the new Vaisala H-Humicap humidity sensor, purportedly accurate to within $\pm$ 2% RH down to -70°C. However, measurements from the field showed the

sensor to regularly "ice up" at temperatures below about -40° (above ~ 300 mb). Therefore, upper-tropospheric humidity data, even from this most recent tropical field experiment, are still lacking.

The COARE mean relative humidity (RH) profile is shown in Fig. 8 (also including a curve for RH with respect to ice above 0°C level). There is a primary peak at low levels at the top of the mixed layer (~ 950 mb) and a secondary peak near 550 mb (near the 0°C level). The latter feature has not

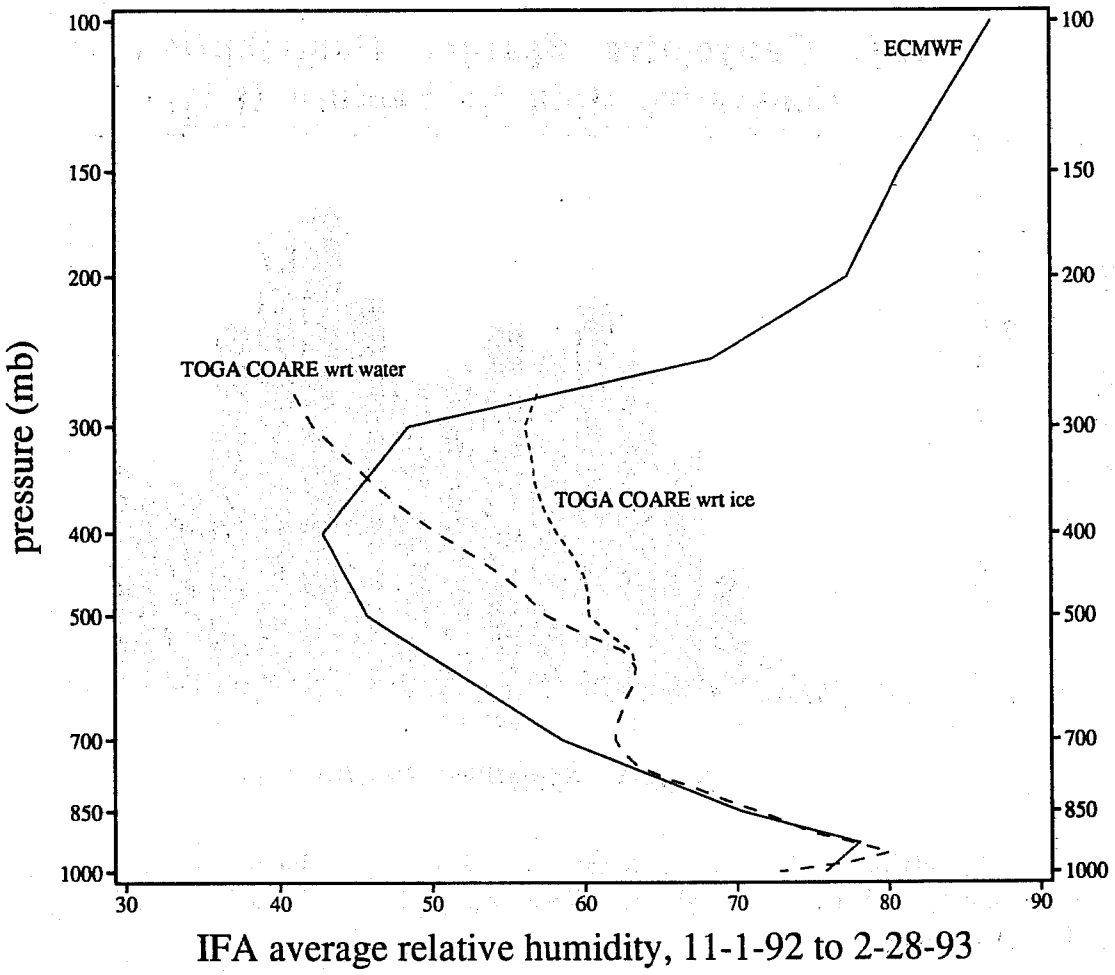

Figure 8: Four-month averages of relative humidity over TOGA COARE Intensive Flux Array from sounding data (with and without ice effects) and ECMWF operational analyses.

received much attention, but can be seen in the climatological studies of Oort (1983), Liu et al. (1991) and Gutzler (1993). It is not present in the ECMWF operational analyses obtained via NCAR (Fig. 8); however, the coarse (~ 100 mb) vertical resolution in the NCAR archive may have precluded its appearance there. The biggest discrepancy between the COARE data and the ECMWF analyses for the four-month period are at midlevels, where ECMWF is much drier. This behavior during COARE has also recently been reported by M. Nuret (Meteo France, personal communication).

To date, explanations for the maximum in RH near 0°C have not yet been offered. One possibility is that deep convection penetrating the stable layers described above could lead to enhanced detrainment and moistening near that level (as described by Bretherton and Smolarkiewicz 1989). Another possibility is that congestus topping out near this level could detrain significant moisture there. A third possibility is that a sufficient number of mesoscale convective systems having attendant stratiform regions with associated "onion-type" soundings (nearly saturated conditions above 0°C, dry below; Zipser 1977) exist in the tropics to perturb the mean relative humidity profile in the manner shown in Fig. 8.

3. CLOUD POPULATIONS

Results from past experiments such as GATE have shown that cell echo areas are log-normally distributed (Lopez 1976, 1977; Houze and Cheng 1977). A thorough review of these studies is found in Houze and Betts (1981). Findings form the recent COARE are not fully in yet, but are expected to be broadly similar. However, as pointed out earlier, careful inspection of cloud size/height statistics for precipitating cloud systems (the tradewind cumulus are generally not precipitating) show departures from smooth distributions (Fig. 7). It is plausible that these departures are related to the recurring stable layers near the 0°C level as these layers inhibit cloud growth (Fig. 6).

An important additional new result from COARE relates to the diurnal cycle of convection. Many studies have reported a late-night or early morning maximum in precipitation over the open ocean, which has been attributed by Gray and Jacobsen (1977) and others to day-night differences in radiative heating in cloudy and cloud-free regions or by Randall et al. (1991) to stabilization during the daytime by shortwave absorption in the free atmosphere.

Ship-based radar data from COARE have confirmed an early morning maximum in precipitation during convectively disturbed periods when mesoscale convective systems and relatively strong winds were prevalent (e.g., the active phase of the 30-60 day or Madden-Julian oscillation [MJO]). These findings are illustrated in Fig. 9a (from T. Rickenbach), which shows the hour-by-hour rain flux for the period. There is almost a 2:1 night-to-day variation in rainflux with a sharp drop-off in precipitation after sunrise and lower values extending into the afternoon. This finding supports the concept that tropospheric radiative effects (above the boundary layer) control the diurnal cycle of convection during this period.

However, during an earlier one-month period characterized by light winds ($<$ 2-3 m s^{-1}) and many smaller convective systems, there was a clear *afternoon* maximum in precipitation (Fig. 9b). During this period, large diurnal variations in sea-surface temperature were observed within the COARE Intensive Flux Array (R. Weller, 1994, personal communication), as has been observed in the past (Lukas 1991), with afternoon SSTs as much as 3°C higher than at night. In sharp contrast to the stronger-wind period, convection during light-wind conditions therefore tends to respond more to boundary-layer diurnal variations, similar to continental regimes. It has recently been shown by Miller

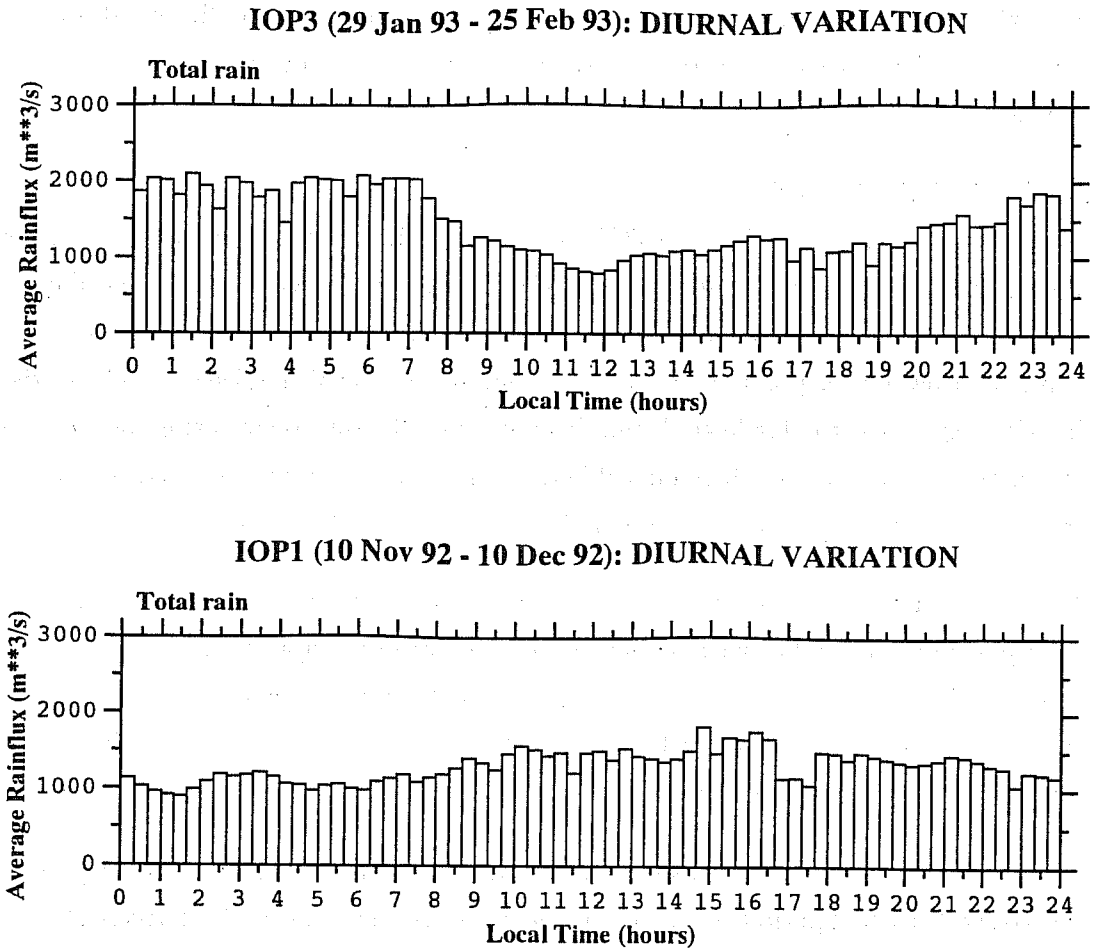

Figure 9: Diurnal variation in rainflux for (a) 29 January - 25 February 1993 and (b) 10 November - 10 December 1992 as measured by MIT radar aboard R/V *Vickers* (courtesy T. Rickenbach).

et al. (1992) that the ECMWF model is particularly sensitive to the surface flux parameterizations in light-wind conditions. As the wind speed goes to zero, fluxes tend to exceed those given by traditional bulk formulae owing to buoyancy effects (e.g., Bradley et al. 1991). The above COARE cloud population statistics suggest that in addition to anomalous behavior in the fluxes in light-wind regimes, dramatic shifts in the diurnal variation of convection over the warm pool are likely to occur accompanying transitions between strong and light wind conditions.

The trade cumulus have already been mentioned as a prominent component of the equatorial cloud population. It is interesting to note that this cloud layer tends to be quite common even in the highly convective region of the warm pool extending across the equator. Reference to Fig. 6 shows that nearly one-third of the soundings contain evidence of the trade cumulus inversion near 800 mb (defined here by lapse rates greater than -4 K km^{-1}), despite being in a region of large-scale mean ascent.

Significant variability in cloud population characteristics can occur on an $\sim$ one-month time scale over the western Pacific warm pool. Infrared satellite images for 6 and 28 December 1992 in Fig. 10 illustrate a dramatic change in the character of the cloud systems – from generally circular structures on the 6th to highly streaked patterns on the 28th. This change in the convective patterns can be explained by referring to a time series of the mean zonal flow over the Intensive Flux Array (IFA; polygon near the center of the satellite images) for the period 1 December 1992 to 15 January 1993 (Fig. 11). Around 6 December the vertical shear through the depth of the troposphere was small ($<$ 5-10 m s^{-1}) whereas during the strong westerly wind burst at the end of December the tropospheric shear exceeded 40 m s^{-1}. The strong upper-level easterly flow during the low-level westerly wind burst contributed to extreme spreading of cirrus from relatively few deep convective systems.

Despite the large areal coverage of the IFA by cirrus on 28 December, the actual rainfall on that date (Day 58) was a local minimum (Fig. 12). IFA rainfall on the 6th (Day 36), when cirrus spreading was minimal, was actually greater. The poor correlation between cirrus coverage and rainfall is confirmed by the considerable overestimation of rainfall for this end-of-December period by the infrared-based Global Precipitation Index (GPI; P. Arkin, personal communication). Comparison of Figs. 11 and 12 shows that the peak in rainfall occurred one to two weeks prior to the peak of the westerly wind burst, consistent with the results of Nakazawa (1988) and others. It is also evident from Fig. 12 that surface evaporation (here computed from the Version I Bulk algorithm prepared for COARE by Fairall/Bradley) does not explain the variability in precipitation: since moisture storage is relatively small, it is controlled primarily by large-scale moisture convergence.

Precipitation computed from the moisture budget (where surface evaporation has been determined using the Fairall/Bradley bulk formula applied to ocean mooring data within the IFA) has been inserted into the heat budget to then obtain the net tropospheric radiative flux divergence as a residual. The results are shown in Fig. 12. The average net tropospheric radiative cooling for the

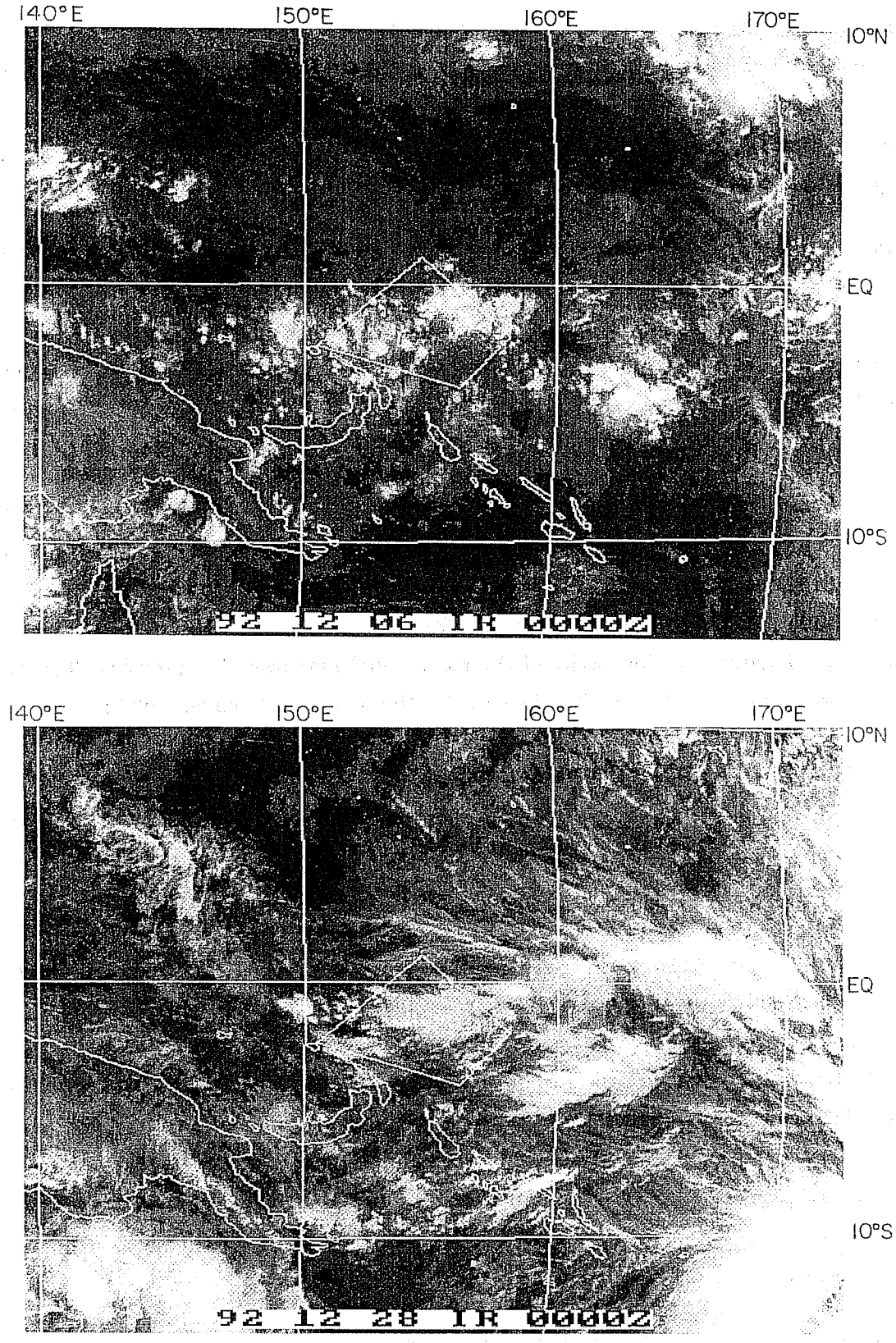

Figure 10: Infrared images from Japaneses GMS satellite for 6 December (top) and 28 December (bottom) 1992. Polygon denotes COARE Intensive Flux Array (IFA).

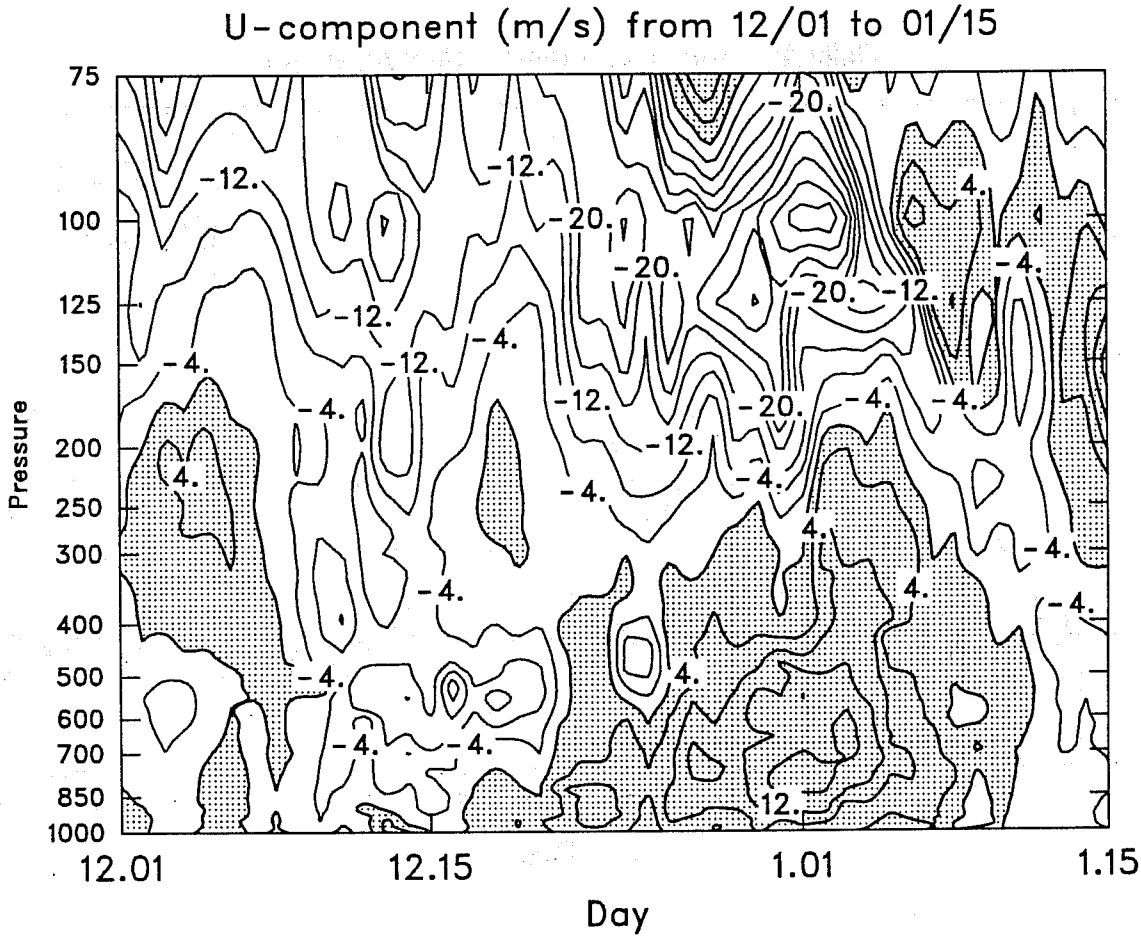

Figure 11: Zonal wind component (m s^{-1}) averaged over COARE IFA from 1 December 1992 to 15 January 1993.

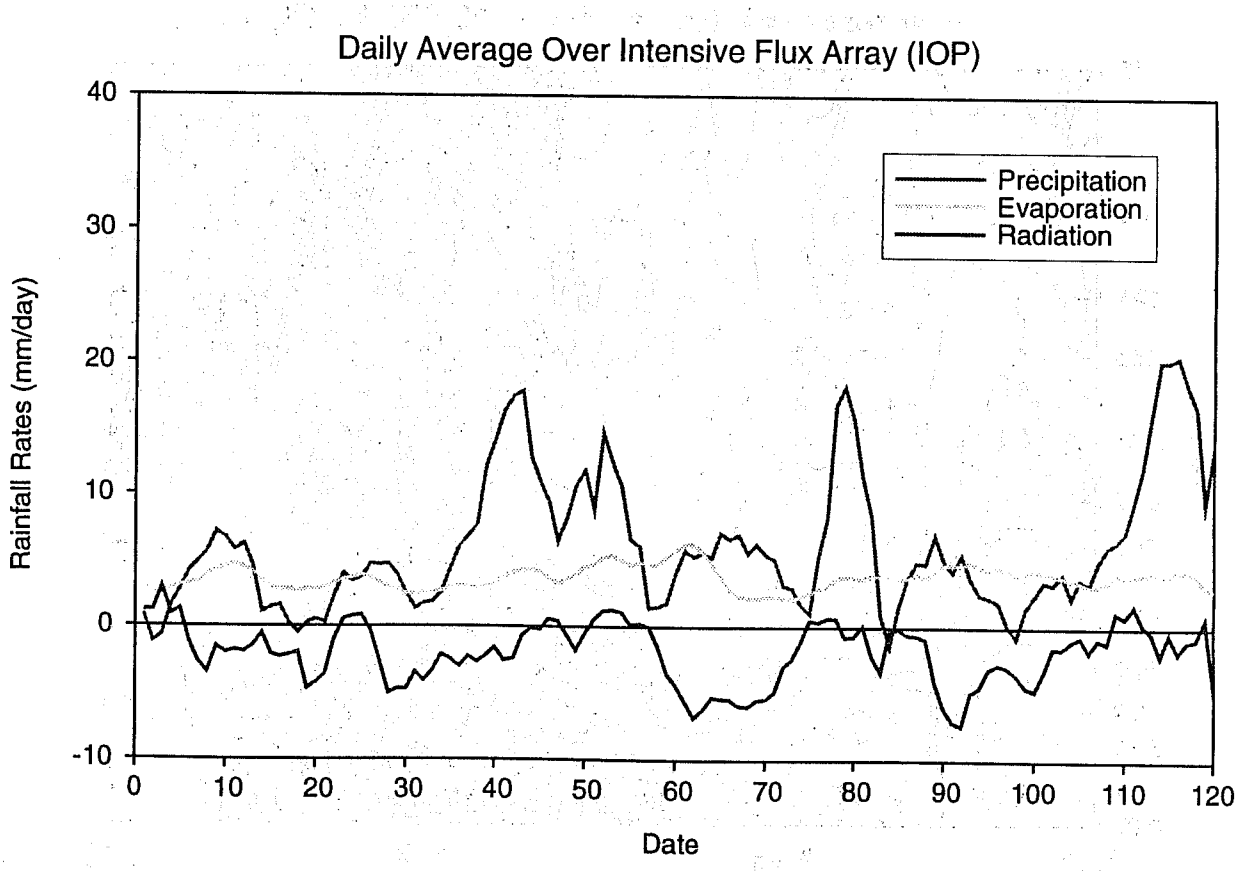

Figure 12: Time series of precipitation, evaporation and radiation in units of mm day^{-1} for COARE IOP. Day 1 corresponds to 1 November 1992 and 120 to 28 February 1993. Three mm day^{-1} roughly corresponds to 1°C day^{-1}.

four-month period was $\sim$ 1°C day^{-1} ($\approx$ 3 mm day^{-1}). At most times there was cooling, but there were several periods when a net tropospheric warming occurred. The end of December is an example. These periods correspond to times of considerable high-level cirrus, but little rainfall, as occurred on 28 December (Fig. 10). The net warming is presumably a result of trapping of longwave emission from the warm ocean by the upper-level cloud layer. These findings highlight complex multiscale interactions occurring over the warm pool whereby low-frequency atmospheric oscillations modulate the tropospheric shear, the altered shear significantly modifies local and regional cloud distributions which, in turn, modify the tropospheric radiative budget. The net tropospheric warming stabilizes the atmosphere, eventually reducing the cloud populations, thereby allowing the sea-surface temperature to recover following its decrease after westerly wind bursts.

4. BOUNDARY-LAYER EFFECTS

Characteristics of mean temperature and moisture fields and cloud distributions have been discussed. Large excursions from these mean structures occur in association with precipitating systems. When precipitation develops, convective downdrafts often occur, which transport cold air to the surface that spreads out over areas much greater than those of the clouds themselves (e.g., Zipser, 1977). During GATE, downdraft-modified boundary layers or "wakes" accompanying precipitating convective systems were found to cover approximately 30% of the total area (Gaynor and Ropelewski 1979). The temperature, moisture and wind stratification within wakes is significantly modified from its structure in undisturbed conditions and recovery of the boundary may take up to $\sim$10 h (Betts 1976; Fitzjarrald and Garstang 1981; Johnson 1981). Locally, surface sensible and latent heat fluxes can be enhanced by an order of magnitude or more in the vicinity of precipitating systems.

An example of the impacts of precipitation downdrafts on the surface sensible and latent heat fluxes associated with a GATE squall line is shown in Fig. 13 (from Johnson and Nicholls 1983). The analyses are based on bulk aerodynamic computations using ship boom data over a 9-h period in the squall-line life cycle. Enhancements in sensible and latent heat fluxes by factors of 10 and 5, respectively, can be seen immediately behind the leading convective line. It can also be seen that the effects of the squall line are felt over an area several hundred km on a side. The collective effects of many of these wakes contribute importantly to the total surface fluxes in disturbed tropical regions.

Since other aspects of the boundary layer are treated elsewhere in this volume (R. Stull), they will not be covered here.

5. CONCLUSIONS

Primary features of the tropical temperature, moisture and cloud distributions have been reviewed. These features should be considered in the validation of cumulus parameterization schemes. It is found that several perturbations to the vertical temperature profile exist in the tropics that are related to distinct cloud populations. The trade inversion layer typically resides between 2 and 3 km and is associated with trade cumulus. Recent results from TOGA COARE and other experiments indicate

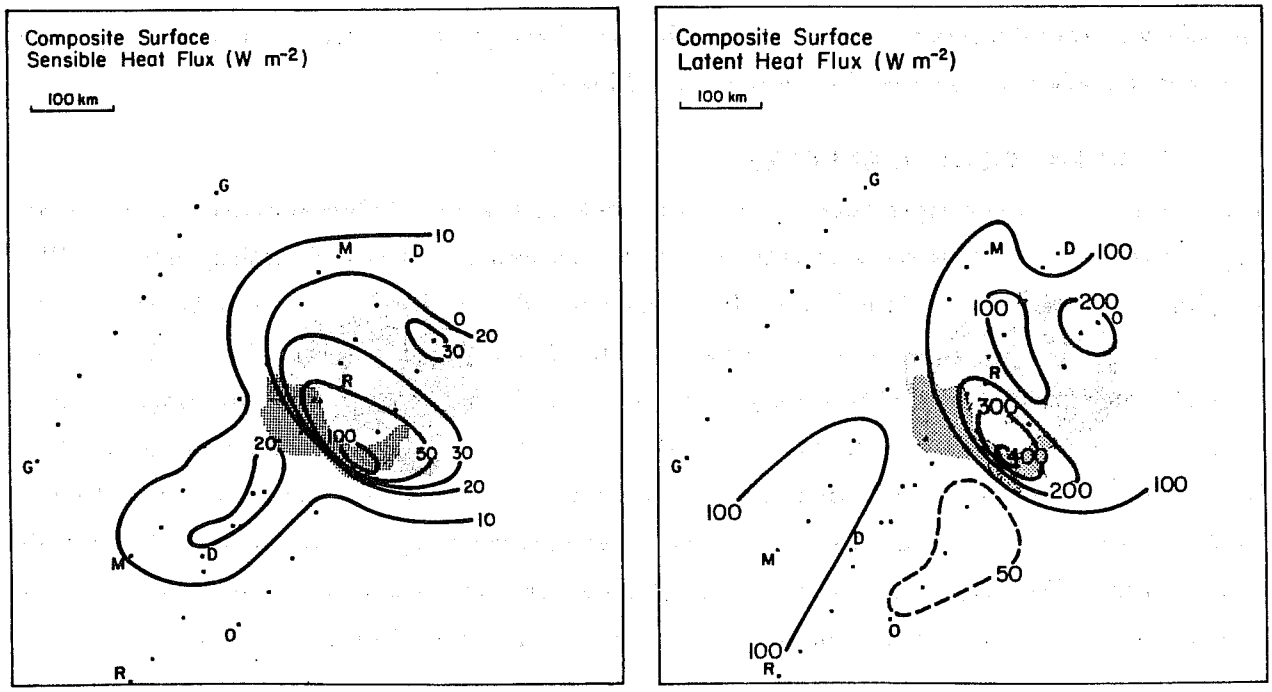

Figure 13: (Left) Composite surface sensible heat flux (W m^{-2}) in region of 12 September 1974 GATE squall-line system. Dark shading refers to leading convective line, and light shading to trailing stratiform region. Hourly positions of *Gilliss* (G), *Meteor* (M), *Dallas* (D), *Researcher* (R), and *Oceanographer* (O) are indicated by dots. (Right) As in top except for composite surface latent heat flux. From Johnson and Nicholls (1983).

that this layer, rather than sloping upward toward the ITCZ, is quasi-horizontal throughout the tropics. This behavior may be a consequence of dynamical rather than thermodynamical processes in the equatorial region.

A relatively new feature in the temperature profile has been identified in TOGA COARE data: a commonly occurring stable layer near the 0°C layer. This layer occurs in a significant fraction of clear-air soundings and is likely a consequence of melting in precipitation regions, local or remote, although the precise mechanisms for its formation are still under investigation.

Much uncertainty exists in the humidity profile in the tropical upper troposphere due to deficiencies in instrumentation. Reliable humidity data above $\sim$ 300 mb are essentially nonexistent. An inversion in the humidity profile is often evident near the 0°C level, as past and recent studies have shown, but has received little attention. Its existence may be related to the stable layer commonly occurring near this level. A possible explanation for the moist layer is detrainment from congestus or cumulonimbus. TOGA COARE data provide evidence of a bimodal distribution of precipitating clouds – one peak in the upper troposphere and another in the midtroposphere. The latter may be associated with the stable layers and moisture inversions near the 0°C level.

6. ACKNOWLEDGMENTS

This research has been supported by the National Oceanic and Atmospheric Administration under Grant NA37RJ0202. Discussions with and the assistance of Paul Ciesielski, Xin Lin, Wayne Schubert, Tom Rickenbach, Jim Bresch, Ken Hart and Pat Haertel are greatly appreciated.

7. REFERENCES

Albrecht, B. A., V. Ramanathan, and B. Boville, 1986: The effects of cumulus moisture transports on the simulation of climate with a general circulation model. *J. Atmos. Sci.*, **43**, 2443-2462.

Betts, A.K., 1976: The thermodynamic transformation of the tropical sub-cloud layer by precipitation and downdrafts. *J. Atmos. Sci.*, **33**, 1008-1020.

Bradley, E.F., P.A. Coppin, and J.S. Godfrey, 1991: Measurements of sensible and latent heat flux in the western equatorial Pacific Ocean. *J. Geophys. Res.*, **96**, 3375-3390.

Bretherton, C.S., and P.K. Smolarkiewicz, 1989: Gravity waves, compensating subsidence and detrainment around cumulus clouds. *J. Atmos. Sci.*, **46**, 740-759.

Cheng, C.-P., and R. A. Houze, Jr., 1979: The distribution of convective and mesoscale precipitation in GATE radar echo patterns. *Mon. Wea. Rev.*, **107**, 1370-1381.

Emanuel, K.A., 1994: *Atmospheric Convection.* Oxford University Press, 580pp.

Findeisen, W., 1940: The formation of the 0°C isothermal layer and fractocumulus under nimbostratus. *Meteorol. Z.*, **57**, 49-54.

Fitzjarrald, D. R., and M. Garstang, 1981: Vertical structure of the tropical boundary layer. *Mon. Wea. Rev.*, **109**, 1512-1526.

Gaynor, J. E., and C. F. Ropelewski, 1979: Analysis of convectively modified GATE boundary layer using in situ and acoustic sounder data. *Mon. Wea. Rev.*, **107**, 985-993.

Gray, W.M., and R.W. Jacobsen, 1977: Diurnal variation of oceanic deep convection. *Mon. Wea. Rev.*, **105**, 1171-1188.

Gutzler, D.S., 1993: Uncertainties in climatological tropical humidity profiles: Some implications for estimating the greenhouse effect. *J. Climate*, **6**, 978-982.

Houze, R.A., Jr., and C.-P. Cheng, 1977: Radar characteristics of tropical convection observed during GATE: Mean properties and trends over the summer season. *Mon. Wea. Rev.*, **107**, 964-980.

Houze, R.A., Jr., and A.K. Betts, 1981: convection in GATE. *Reviews of Geophysics and Space Physics*, **19**, 541-576.

Johnson, R.H., 1981: Large-scale effects of deep convection on the GATE tropical boundary layer. *J. Atmos. Sci.*, **38**, 2399-2413.

Johnson, R.H., 1986: Implications of lower-tropospheric warming and drying in tropical mesoscale convective systems for the problem of cumulus parameterization. *J. Meteor. Soc. Japan*, **64**, 721-726.

Johnson, R.H., and M. E. Nicholls, 1983: A composite analysis of the boundary layer accompanying a tropical squall line. *Mon. Wea. Rev.*, **111**, 308-319.

Johnson, R.H., J.F. Bresch, P.E. Ciesielski and W.A. Gallus, Jr., 1993: The TOGA/COARE atmospheric sounding array: Its performance and preliminary scientific results. Preprints, 20th Conference on Hurricanes and Tropical Meteorology, San Antonio, TX, 10-14 May, pp. 1-4.

Liu, W.T., W. Tang, and P.P. Niiler, 1991: Humidity profiles over the ocean. *J. Climate*, **4**, 1023-1034.

Lopez, R.E., 1976: Radar characteristics of the cloud populations of tropical disturbances in the northwest Atlantic. *Mon. Wea. Rev.*, **104**, 268-283.

Lopez, R.E., 1977: The lognormal distribution and cumulus cloud population. *Mon. Wea. Rev.*, **105**, 1865-1872.

Lukas, R., 1991: The diurnal cycle of sea surface temperature in the western equatorial Pacific. *TOGA Notes*, **2**, 1-5.

Mapes, B.E., 1993: Gregarious tropical convection. *J. Atmos. Sci.*, **50**, 2026-2037.

Miller, M.J., A.C.M. Beljaars, and T.N. Palmer, 1992: The sensitivity of the ECMWF model to the parameterization of evaporation from the tropical oceans. *J. Climate*, **5**, 418-434.

Nakazawa, T., 1988: Tropical super clusters within intraseasonal variations over the west Pacific. *J. Meteor. Soc. Japan* **66**, 777-786.

Nicholls, M.E., R.A. Pielke, and W.R. Cotton, 1991: Thermally forced gravity waves in an atmosphere at rest. *J. Atmos. Sci.*, **48**, 1869-1884.

Oort, A.H., 1983: *Global atmospheric circulation statistics, 1958-1973.* NOAA Professional Paper 14, Rockville, MD, NOAA, U.S. Department of Commerce, 180pp.

Payne S.W., and M.M. McGarry, 1977: The relationship of satellite inferred convective activity to easterly waves over west Africa and the adjacent ocean during Phase III of GATE. *Mon. Wea. Rev.*, **105**, 413-420.

Randall, D. A., Harshvardan and D. A. Dazlich, 1991: Diurnal variability of the hydrological cycle in a general circulation model. *J. Atmos. Sci.*, **48**, 40-62.

Raymond, D.J., and H. Jiang, 1990: A theory for long-lived mesoscale convective systems. *J. Atmos. Sci.*, **47**, 3067-3077.

Reed, R. J., and E. E. Recker, 1971: Structure and properties of synoptic-scale waves disturbances in the equatorial western Pacific. *J. Atmos. Sci.*, **28**, 1117-1133.

Schubert, W.H., P.E. Ciesielski, C. Lu, and R.H. Johnson, 1994: Dynamical adjustment of the trade wind inversion layer. *J. Atmos. Sci.*, (submitted)

Webster, P.J., and R. Lukas, 1992: The TOGA Coupled Ocean-Atmosphere Response Experiment. *Bull. of the Amer. Meteor. Soc.*, **73**, 1377-1416.

Zipser, E.J., 1977: Mesoscale and convective-scale downdrafts as distinct components of squall-line structure. *Mon. Wea. Rev.*, **105**, 1568-1589.